Impacts of Hurricane Storm Surge on Infrastructure Vulnerability for an Evolving Coastal Landscape

Katherine A. Anarde, S.M.ASCE[1]; Sabarethinam Kameshwar, A.M.ASCE[2]; John N. Irza[3]; Jeffrey A. Nittrouer, Ph.D.[4]; Jorge Lorenzo-Trueba, Ph.D.[5]; Jamie E. Padgett, Ph.D., P.E., A.M.ASCE[6]; Antonia Sebastian, Ph.D., S.M.ASCE[7]; and Philip B. Bedient, Ph.D., P.E., F.ASCE[8]

Abstract: Predicting coastal infrastructure reliability during hurricane events is important for risk-based design and disaster planning, including delineating viable emergency response routes. Previous research has focused on either infrastructure vulnerability to sea-level rise and coastal flooding, or the impact of changing sea level and landforms on surge dynamics. This paper represents a multidisciplinary effort to provide an integrative model of the combined impacts of sea-level rise, landscape changes, and coastal flooding on the vulnerability of highway bridges—the only access points between barrier islands and mainland communities—during extreme storms. Coastal flooding is forward modeled for static projections of geomorphic change. First-order parameters that are adjusted include sea level and land surface elevation. These parameters are varied for each storm simulation to evaluate relative impact on the performance of bridges surrounding Freeport, Texas. Vulnerability is estimated by evaluating both the probability of structural failure given surge and wave loads as well as the time inundated. The probability of bridge failure is found to increase with storm intensity and sea level because bridge fragility increases with storm surge height. The impact of a shifting landscape on bridge accessibility is more complex; barrier island erosion and transgression can increase, decrease, or produce no change in inundation times for storms of different intensity due to changes in wind-setup and back-bay interactions. These results suggest that tying down bridge spans and elevating low-lying roadways approaching bridges may enhance efforts aimed at protecting critical infrastructure. **DOI: 10.1061/(ASCE)NH.1527-6996.0000265.**

Author keywords: Bridges; Storm surge fragility; Sea-level rise; Barrier island; Coastal erosion; *ADVanced CIRCulation (ADCIRC)*; *Simulating WAves Nearshore (SWAN)*.

Introduction

The performance of transportation infrastructure during hurricane events is crucial for evacuation and poststorm recovery operations. When bridges become inaccessible, whether through loss of structural integrity or sustained high water, disaster response activities are jeopardized. Identifying the major sources of risk to coastal infrastructure is therefore vital for disaster prevention and mitigation efforts. As development and population of coastal landscapes continue to grow (Neumann et al. 2015), despite accelerated rates of global sea-level rise (DeConto and Pollard 2016) and uncertainties in future flood risk (Church et al. 2013), there is tremendous need to understand the safety and security of coastal infrastructure.

Storm surge and wave-induced loading are the dominant threat to the safety of bridges during hurricanes (Kameshwar and Padgett 2014; Padgett et al. 2008). When the level of storm surge and waves rises to or above the bottom of the bridge deck, the deck is subjected to uplift and can thereafter be shifted or completely displaced. This mode of failure was ascribed to the damage or destruction of 26 bridges during Hurricane Ike, which struck the Houston-Galveston region of Texas in September 2008 (Stearns and Padgett 2011). Bridge deck unseating was also observed at nearly 1,000 bridge spans in Louisiana, Alabama, and Mississippi after Hurricane Katrina in 2005 (Padgett et al. 2012). Bridge infrastructure reliability during hurricane events extends beyond structural integrity; elevated water levels due to inland flooding and deposits of debris can likewise prolong the downtime of major transportation networks (Padgett et al. 2008).

In learning from Hurricane Ike and other recent natural disasters, risk assessment frameworks have been developed to quantify bridge infrastructure vulnerability to hurricane-induced wave and surge loads (Ataei and Padgett 2013; Kameshwar and Padgett 2014). In addition to these tools, regional managers and stakeholders need information on future flood risk to effectively manage infrastructure systems. This becomes increasingly complex given uncertainties due to climate and environmental changes, which impact, for example, cyclone climatology, sea-level rise, and coastal morphology. These dynamic conditions render low-lying

[1]Ph.D. Student, Dept. of Civil and Environmental Engineering, Rice Univ., 6100 Main St. MS-317, Houston, TX 77005 (corresponding author). E-mail: kanarde@rice.edu

[2]Ph.D. Candidate, Dept. of Civil and Environmental Engineering, Rice Univ., Houston, TX 77005. E-mail: sk56@rice.edu

[3]Graduate Student, Dept. of Civil and Environmental Engineering, Rice Univ., Houston, TX 77005. E-mail: jni1@rice.edu

[4]Assistant Professor, Dept. of Earth Science, Rice Univ., Houston, TX 77005. E-mail: nittrouer@rice.edu

[5]Assistant Professor, Dept. of Earth and Environmental Studies, Montclair State Univ., Montclair, NJ 07043. E-mail: lorenzotruej@montclair.edu

[6]Associate Professor, Dept. of Civil and Environmental Engineering, Rice Univ., Houston, TX 77005. E-mail: jamie.padgett@rice.edu

[7]Postdoctoral Researcher, Dept. of Civil and Environmental Engineering, Rice Univ., Houston, TX 77005. E-mail: ags3@rice.edu

[8]Professor, Dept. of Civil and Environmental Engineering, Rice Univ., Houston, TX 77005. E-mail: bedient@rice.edu

Note. This manuscript was submitted on December 23, 2016; approved on May 25, 2017; published online on October 26, 2017. Discussion period open until March 26, 2018; separate discussions must be submitted for individual papers. This paper is part of the ***Natural Hazards Review***, © ASCE, ISSN 1527-6988.

coasts particularly vulnerable to extreme flood events (Cazenave and Cozannet 2014; Woodruff et al. 2013).

Hydrodynamic models have been used extensively to study the impacts of relative sea-level rise (SLR), which includes eustatic sea-level rise and local seafloor elevation changes due to isostatic and sediment compaction effects (Church et al. 2013), on coastal flooding (Atkinson et al. 2013; Bilskie et al. 2014, 2016a; Ding et al. 2013; Mousavi et al. 2011; Passeri et al. 2015a; Ratcliff and Smith 2012; Smith et al. 2010; Wang et al. 2012; Zhang et al. 2013). Results from these studies show that hurricane storm surge flooding under SLR can be linear (spatiotemporally consistent) or nonlinear, because it is influenced by local variability in coastal topography, land-use, and/or storm characteristics. However, most of these studies simulated flooding of present-day coastal landforms and did not incorporate morphodynamic modifications to coastal landscapes, which have the potential to alter storm hydrodynamics.

Recent investigations have shifted toward a synergistic approach in modeling the effects of SLR by incorporating the interactions between physical and ecological environments in hydrodynamic simulations (Bilskie et al. 2016a; Cobell et al. 2013; Ferreira et al. 2014; Passeri et al. 2015a, b, 2016). For example, Passeri et al. (2015a) evaluated the sensitivity of a high-resolution tide, wave, and hurricane storm surge model to projected shoreline and nearshore morphology changes associated with SLR for the Florida Panhandle. Bilskie et al. (2016a) expanded upon this work by incorporating changes in barrier island morphology, land use land cover (LULC), and salt marsh evolution across Mississippi, Alabama, and the Florida Panhandle. Both studies found that, when combined with SLR, erosional landscape changes modified storm surge and wave dynamics by enhancing flooding of back-bay regions, thereby amplifying surge, wave heights, and inundation extent inland of deflated barriers. The results of these studies demonstrate that hydrodynamic responses to SLR are complex and spatially variable, particularly when influenced by local landscape changes.

Existing scientific approaches that evaluate infrastructure vulnerability have not considered the combined effects of rising seas and changing coastal landscapes; the unique feature of this study is to model both of these environmental changes to determine the safety and accessibility of coastal bridges. This paper presents a novel approach which couples hydrodynamic and geomorphic modeling frameworks (e.g., Bilskie et al. 2016a) with engineering reliability analysis of physical infrastructure. The study area centers on Brazoria County, Texas (Fig. 1), a wave-dominated microtidal environment that has endured numerous powerful hurricanes, including Alicia (1983) and Ike (2008). This portion of the upper Texas Gulf Coast (UTGC) was strategically selected because of its ecologically diverse and low-lying landscape, which is heavily developed for recreation, trade, and commerce. The western half of the study area is composed of the Brazos River delta and the City of Freeport, an important industrial center and deep-water port. A system of levees and pump stations protect a 109-km^2 area encompassing Freeport and surrounding industrial complexes (U.S. Army Corps of Engineers 2005). To the east stretches Follets Island, a narrow barrier spit backed by lagoons that connect to the Gulf of Mexico via San Luis Pass, a microtidal inlet. The shoreline along this portion of the UTGC is characterized by rapid retreat (1.5–3.9 m/year) which is attributed to accelerated rates of SLR, punctuated storm impacts, and diminished sediment supply (Morton et al. 2004; Wallace and Anderson 2013; Wallace et al. 2009). This long-term regional recessional trend is incorporated

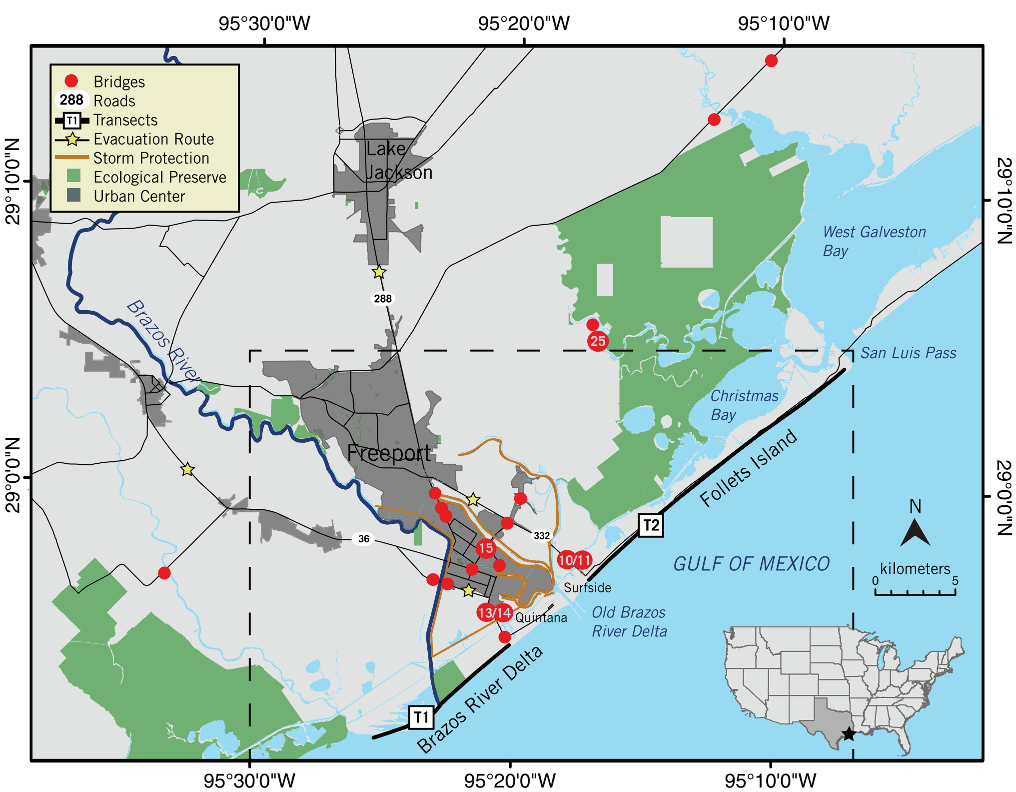

Fig. 1. (Color) Map of Freeport, Texas, showing features of the natural and developed landscape relevant to this study, including contributing rivers, bays, ecological preserves, significant roads, bridges, evacuation routes, and storm protection systems; the transect locations used to analyze storm surge are also shown; the dashed box outlines the area depicted in Figs. 2 and 6

into the current study via modifications to shoreline, barrier island, and deltaic morphology, and by considering an intermediate SLR scenario for the year 2050. A hydrodynamic storm surge and wave model is used to simulate a suite of synthetic and historical storms for present and projected future conditions. Bridge vulnerability assessment is performed, encompassing both the structural fragility and prehurricane and posthurricane accessibility, for a portfolio of bridges critical for transportation in this region. The study concludes with performance assessments of regional transportation infrastructure and provides feedback for planning risk management strategies.

Methods

Wave and Storm Surge Model

The evolution of storm surge and waves is simulated along the UTGC for various storms and climate change scenarios using the tightly coupled *Simulating WAves Nearshore* and *ADVanced CIRCulation* ($SWAN + ADCIRC$) model (Dietrich et al. 2011; Luettich and Westerink 2004). The coupling of $SWAN$ and $ADCIRC$ allows for computation of water levels, depth-averaged currents, and wave action density on a single mesh consisting of nonoverlapping, unstructured triangular elements. The fidelity of the $SWAN + ADCIRC$ model for simulating storm surge and waves along the UTGC was validated for Hurricane Ike by Hope et al. (2013) using an extensive collection of measured wave and water levels across the region. This study utilizes the TX2008r35h mesh, an improved version of the computational domain used by Hope et al. (2013) that incorporates local mesh refinements along the Texas coastline. The TX2008r35h mesh comprises 6.67 million triangular elements that are discretized to extend resolution of complex coastal features from 100 to 200 m in the nearshore environment down to 20 m within channels and levees (Dietrich et al. 2013). Bathymetric values are representative of post-Ike conditions and were obtained from multiple data sources outlined by Hope et al. (2013). This study modifies the TX2008r35h mesh to represent projected geomorphic change under a future SLR scenario for ca. 2050, as detailed in the section "Evolving Coastal Morphology and Sea-Level Rise." Astronomical tides are neglected in numerical simulations in order to isolate the impact of meteorological forcing on SLR. Therefore storm surge is defined as the hurricane still-water level driven by wind, wave, and pressure setup.

Storm Selection

$SWAN + ADCIRC$ has been used extensively to understand storm hydrodynamics in the greater Houston-Galveston region through simulation of historical storms (Dawson et al. 2011; Hope et al. 2013) and variations thereof (Sebastian et al. 2014). However, the scarcity of regional historical hurricane records has limited analysis of how local hydrodynamics covary with storm attributes. Synthetic wind and pressure fields have been used to quantify the influence of storm size on surge generation (Irish et al. 2008) and evaluation of flood hazards (Vickery and Blanton 2008; Toro 2008). With the development of the joint probability method with optimal sampling (JPM-OS), hundreds of synthetic storms with varied physical attributes (e.g., radius to maximum winds, maximum wind speed, minimum pressure, and angle of approach) can be simulated for any storm track using $SWAN + ADCIRC$.

For this study, three storms were selected from the FEMA suite of 162 JPM-OS–derived synthetic hurricanes for the UTGC (FEMA and USACE 2011) to explore the relative impact of storm intensification on storm surge and wave generation. These synthetic storms were identified as proxies for wind fields that exhibit low, medium, and high potential for storm surge generation as indicated by the storm's integrated kinetic energy (IKE) value, an alternative metric to the Saffir-Simpson scale for storm intensity (Powell and Reinhold 2007). The IKE index allows for the inclusion of storm size, a critical factor in the generation of large storm surges (Irish et al. 2008), in assessing hurricane destruction potential. Integrated kinetic energy has been shown to have a strong correlation to peak storm surge as well as to the regional surge response (Bass et al. 2017). The IKE index is calculated as the sum of kinetic energy per unit volume over the storm domain volume (V) as

$$\mathrm{IKE_{TS}} = \int_v \frac{1}{2}\rho U^2 dV \tag{1}$$

where U = surface wind velocity (m/s) at 10 m above mean sea level for tropical storm–force winds (>18 m/s); and ρ = density of air. This value is commonly expressed in terajoules (TJ) and represents a storm's kinetic energy at landfall. The synthetic storms chosen for this study exhibited the lowest, median, and highest IKE within the subgroup of FEMA storms that follow a comparable angle of approach to Hurricane Ike (Table 1) and are hereafter referred to as the small (S), medium (M), and large (L) storms. Hurricane Ike's IKE value, as calculated by the National Hurricane Center, represents an upper limit for this study and is therefore referred to herein as the extra-large (XL) storm. All four storms were shifted in space such that landfall occurred ∼40 km southwest of Freeport, Texas, the industrial epicenter of Brazoria County (Fig. 1). This landfall location was selected because it produced the maximum storm surge at the bridge locations relative to other storms tracks simulated during sensitivity modeling. Table 1 illustrates the variability of meteorological attributes for the modeled storms including maximum wind speed ($U_{\max}$), radius to maximum winds ($R_{\max}$), radius to tropical storm–force winds (R_{TS}, $U > 18$ m/s), radius to hurricane-force winds (R_H, $U > 33$ m/s), minimum barometric pressure ($P_{\min}$), 6-h forward speed at landfall (V_f), and angle of approach (α_{app}, degrees from due north).

Evolving Coastal Morphology and Sea-Level Rise

Because of the complex nature of coastal processes operating over a wide range of timescales, there is no universal model for assessing the impact of SLR on coastal morphology (Cazenave and Cozannet 2014; FitzGerald et al. 2008). Instead, a technique that is typically

Table 1. Meteorological Parameters and Storm Surge Index for Selected Storms Making Landfall at Freeport, Texas

Storm name	Storm identifier	$U_{\max}$ (m/s)	$R_{\max}$ (km)	$P_{\min}$ (mb)	α_{app} (degrees)	R_{TS} (km)	R_H (km)	6-h V_f (m/s)	$\mathrm{IKE_{TS}}$ (TJ)
Small	FEMA 37	54.3	17	960	−41	187	61	6.7	25
Medium	FEMA 38	40.9	41	975	−41	329	96	6.7	52
Large	FEMA 30	37.2	62	978	−41	407	109	6.7	76
Extra-large	Hurricane Ike (2008)	48.7	59	952	−36	479	159	5.0	99

Nat. Hazards Rev., 2018, 19(1): 04017020

applied as a first-order estimate to predict movement of beaches and barriers in response to SLR and storms is to extrapolate historical trends of the shoreface (Passeri et al. 2015a; Ranasinghe et al. 2012). This study estimated a future geomorphic condition for the year 2050 by imposing modern rates of shoreline and bayline migration measured at Follets Island. Over the last 30 years, shoreline migration (1.5–3.9 m/year) has been faster than bayline accretion (<1 m/year) (Gibeaut et al. 2003; Paine et al. 2012). The mechanism behind this trend has been linked to a diminishing regional sand supply (Morton et al. 2004, 2005; Wallace and Anderson 2013) and deposition of a significant portion (~38%) of sediment overwash into the back-barrier bay (Odezulu et al. 2017). Acoustic backscatter from compressed high-intensity radar pulse (CHIRP) surveys conducted after Hurricane Ike show that there is no sand below ~4 m water depth to the ravinement surface at ~8–10 m (Carlin et al. 2015). Sediment availability in the upper shoreface is also extremely limited, because the upper shoreface contains no more than 1.5 m of sand (Odezulu et al. 2017). This, in conjunction with ample back-barrier accommodation space (three times the volume of the barrier), limits poststorm recovery of the dune line and barrier-island rollover processes. Therefore Follets Island is becoming lower and narrower, which will likely lead to higher overwash fluxes (Schwartz 1975; Rosati et al. 2006; FitzGerald et al. 2008; Park and Edge 2011) and potentially complete submergence due to accelerated sea-level rise (Odezulu et al. 2017).

This study used average shoreline (2.7 m/year) and bayline (0.5 m/year) migration rates to model the landward displacement of Follets Island for the year 2050. Based on the barrier island configuration in 2008, when bathymetry data used in this study were collected, the resulting shoreline and bayline displacement values are 113 and 20 m [Fig. 2(a)]. These are intermediate (average) values when considering the total range based on the measured annual retreat rates (i.e., 63–164 m landward shoreline retreat for 2050). Shoreface retreat, however, is nonlinear and dependent on punctuated storm conditions; for example, after Hurricane Ike, parts of Follets Island eroded up to 180 m (Carlin et al. 2015; Harter et al. 2015). This study assumed that shoreface movement preserves the equilibrium shape profile and therefore that the associated transgressive ravinement of the beach profile occurs to the depth of closure, 8–10 m, so that the subaqueous shoreface is leveled to this depth (Wallace et al. 2010). Additionally, the subaerial extent of the barrier was lowered to 0.5 m above mean sea level (AMSL) to account for erosion by storm overwash due to narrowing of the barrier island.

The Brazos River delta (subaqueous and subaerial) was similarly modified. In its current configuration, the morphology is that of a classic wave-dominated system [Fig. 2(b)]. Sediment feeding this delta is primarily mud (~80%), with some sand (~20%), whereby much of the discharge arises during decadal (punctuated) flood events. The morphology of the delta nevertheless remains relatively unimpacted even during prolonged low-flow conditions (i.e., droughts) because the shoreface is stabilized by significant volumes of large woody debris that attenuates wave energy. This wood is continuously discharged by the Brazos River, even during low flow (Huff 2015). Relative sea-level rise threatens this delta, however, and the system remains quite vulnerable to removal via erosion. History provides a prime example: the location of the modern Brazos delta is a manifestation of displacement of the main channel by the U.S. Army Corps of Engineers in 1929 to facilitate maintenance of the Freeport deep-water navigation channel. The old delta, without supply of wood and sediment, rapidly deteriorated in the energetic wave climate of the Gulf of Mexico, and was completely eroded to a depth of 8 m within 13 years of the engineered diversion (Fraticelli 2006).

The tidal inlet geometry at San Luis Pass was not modified for a changing tidal prism because both lobes are stabilized due to engineering practices: the downdrift lobe is developed with residential properties and the updrift lobe provides structural support for a bridge that crosses the inlet. Future changes in LULC and marsh evolution were also neglected for the 2050 scenario because it has been demonstrated that the effects of bottom roughness on storm surge are minor compared with the effects of SLR along the UTGC (Atkinson et al. 2013). However, Manning's roughness coefficients (surface friction) were altered for newly wetted areas due to changes in geomorphology. Lastly, changes to regional storm protection features (e.g., raising existing levees or constructing of storm gates), although having the potential to alter inundation patterns, were likewise not included in the 2050 scenario because they are presently not detailed in terms of design or implementation.

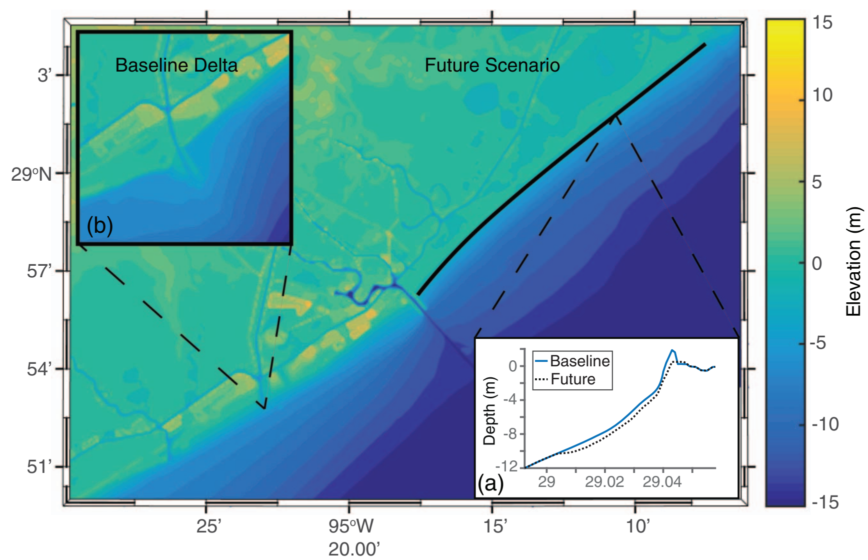

Fig. 2. (Color) Bathymetric and topographic representation of the modeled landscape changes for 2050 (future scenario) within the study area; subplots indicate 2008 (baseline scenario) morphologies for (a) Follets Island (for a representative cross-shore profile) and (b) the Brazos River delta

In any case, with the exception of one bridge, the infrastructure highlighted in this study is located outside the region in which protection system modifications are recommended (Gulf Coast Community Protection and Recovery District 2016).

The global sea-level change projections developed by Parris et al. (2012) for use in coastal vulnerability studies were locally calibrated by adjusting for vertical land motion (VLM). This was accomplished using the U.S. Army Corps of Engineers sea-level change curve calculator, which can estimate VLM through decomposition of mean sea-level data from long-term tide gauge records (Zervas et al. 2013; USACE 2015). The regional mean sea-level trend in Freeport, Texas, is 4.43 ± 1.05 mm/year (NOAA 2016) based on monthly sea-level data collected between 1972 and 2008. The VLM-adjusted SLR scenarios for 2050 (relative to 2008) in Freeport range 0.22–0.7 m. Because an intermediate rate of shoreline (and bayline) migration was chosen for the geomorphic change projection, the intermediate-low SLR scenario, 0.31 m, was selected for consistency.

The twelve simulations conducted in this study incorporated four storm intensities (S, M, L, and XL), two imposed sea levels 0) and 0.31 m AMSL), and two coastal morphology configurations [2008 (baseline) and 2050]. Each storm was simulated for three scenarios: (1) baseline (0 AMSL and 2008 morphology); (2) future morphology (FM) (0 AMSL and 2050 geomorphic projection); and (3) future scenario (FM + SLR) (0.31 m AMSL and 2050 geomorphic projection). The morphological changes modeled in this study are intrinsically linked to SLR and therefore the FM scenario should only be used for comparative analysis because it does not represent a precise future condition.

Bridge Infrastructure Performance Assessment

The hydrodynamics at 25 bridges located within Brazoria County (Fig. 1) were examined for each of the 12 storm surge and wave simulations. A bridge was selected for analysis if it met the following criteria: (1) bridge is on an arterial roadway, (2) bridge is proximate to the coastline or water body with a hydraulic connection to the coast, or (3) the bridge is the sole access point to a community. The dominant failure mode was bridge deck unseating due to storm surge and wave attack at either the bridge approach span (AS) or main span (BS). The bridge approach spans are akin to ramps that connect the roadway to the main bridge span. Although the failure modes may differ in location (AS or BS) between bridges, for simplicity, both locations are collectively referred to herein as the bridge span. The bridge spans in this study were all simply supported; this superstructure type is particularly vulnerable to bridge deck unseating. Table 2 specifies the location of failure (AS or BS) for key bridges discussed in this study.

Bridge details were extracted from bridge plans obtained from the Texas Department of Transportation and the Office of the Brazoria County Engineer. For this study, bridges were classified based on the elevation of the roadway approaching the bridge (hereafter referred to simply as the roadway) and proximity to the coast. The roadway elevation, which was incorporated into $SWAN + ADCIRC$ as the ground elevation, was extracted for each bridge from the nearest $SWAN + ADCIRC$ node. Bridges were deemed low-lying if the roadway elevation was less than 0.5 m (Table 2).

Stage hydrographs generated from $SWAN + ADCIRC$ allow for comparison of maximum inundation depths above the roadway (henceforth referred to as roadway inundation) and duration of roadway inundation between scenarios. This analysis then informs a probabilistic assessment of bridge failure due to surge and wave loading. Maximum inundation depth provides a perspective on the magnitude of the hazard whereas time of roadway inundation quantifies the bridge accessibility. Probability of failure likewise quantifies the vulnerability of bridges to hurricane attack and dictates the long-term availability of a bridge after a storm. To relate the hydrodynamics observed at bridge locations to trends along the coast, changes in volumetric flow and significant wave height were analyzed across the modeled landscape changes.

Hydrodynamics

Stage hydrographs were generated for each bridge location by extracting water surface elevations from the nearest land-based $SWAN + ADCIRC$ node to the bridge approach span or main span for each time step in the storm simulations (Fig. 3). Water surface elevations were temporally synchronized during postprocessing by shifting the time of landfall for the baseline synthetic storms (S, M, and L) to match Hurricane Ike (XL). Water surface elevations were converted to stage by subtracting the elevation of the nearest node such that the water level could be interpreted as the depth of inundation or residual storm surge (neglecting waves and tides) above the roadway. The threshold for roadway inundation (black line in Fig. 3), and therefore bridge accessibility, was set at 0.6 m (~2 ft), which is the approximate depth at which most vehicles become buoyant in flood waters (National Weather Service 2016). The duration of roadway inundation was calculated as the cumulative time over the simulated storm that water levels remained above this threshold.

To assess whether and how localized trends in relative storm surge elevations are influenced by the large-scale changes to coastal morphology and SLR, the surge response at the coastline was examined by computing the volumetric flow across discrete linear transects (solid black lines in Fig. 1). The two transects discussed herein produced large changes in system hydrodynamics and encompassed the morphological modifications to the coast. Transects were created in *ArcGIS* and populated with equidistant nodes spaced 50 m apart. Water surface elevations, velocities, and bathymetric data were extracted for each transect node from

Table 2. Characteristics of Selected Vulnerable Bridges

Bridge identifier	Node elevation (m AMSL)	Study classification	Susceptible spans	Super-structure type	Bridge clearance, H_B (m)	Normal water depth (m)
10	0.388	LC	AS	SS	3.1	0
11	0.432	LC	AS	SS	3.1	0
13	1.901	EC	AS	SS	2.1	0
14	0.648	EC	AS	SS	2.1	0
15	2.356	EI	BS	SS	4.7	4.3
25	0.462	LI	BS	SS	2.0	3.3

Note: AMSL = above mean sea level; AS = approach span; BS = bridge span; EC = elevated coastal; EI = elevated inland; LC = low-lying coastal; LI = low-lying inland; SS = simply supported.

Nat. Hazards Rev., 2018, 19(1): 04017020

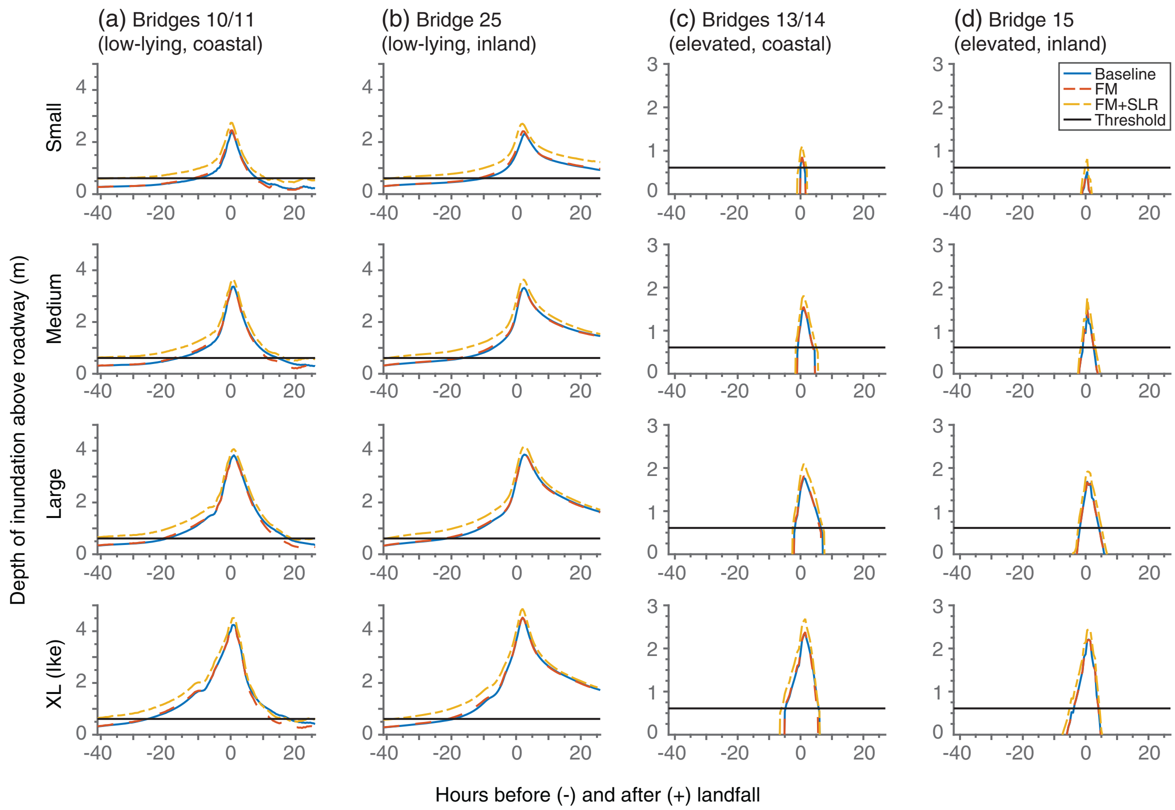

Fig. 3. (Color) Stage hydrographs representing depth of roadway inundation at selected bridges (a–d) for all modeled scenarios (line type) and storm intensities (rows); the black line indicates the threshold of roadway inundation, beyond which the bridge is deemed inaccessible; note that inundation depth is scaled separately for low-lying (Bridges 10, 11, and 25) and elevated bridges (Bridges 13, 14, and 15)

the nearest *SWAN + ADCIRC* node to calculate volumetric flow, which was then integrated along the transect length. Wave dissipation across the modified landscape was also evaluated by differencing maximum significant wave heights for different scenarios.

Probability of Failure

The probability of structural failure, via bridge deck unseating, was evaluated for each bridge using a parameterized bridge fragility function developed by Kameshwar and Padgett (2014), which gives the conditional probability of failure for a given inundation depth (S), wave height (H), and bridge clearance (H_B) as

$$p(\mathrm{fail}|S,H,H_B) = \frac{1}{(1+\exp(-l_x))} \tag{2}$$

where l_x = polynomial representing the logarithm of odds in favor of bridge failure

$$l_x = 2.71 + 3.47(H_B - S) - 1.59H - 0.17H(H_B - S) + 0.22(H_B - S)^2 - 0.05H^2 \tag{3}$$

The polynomial l_x consists of a nonlinear combination of the predictor variables S, H, and H_B with coefficients estimated by minimizing the deviance of the logistic regression model in Eq. (2). The wave height (H) in Eq. (3) is a random variable which can take all possible values of wave height for a given storm surge elevation. The probability of observing different instances of wave heights (h) is characterized by the probability density function of wave heights—$f_{(H)}(h)$. The probability density function $f_{(H)}(h)$ was obtained using an empirical formulation described by Elfrink et al. (2006) with significant wave heights (H_s) from *SWAN + ADCIRC* as input. This provided the opportunity to weigh the failure probability calculated using Eqs. (2) and (3) with the probability of observing a given wave height (h)

$$p(\mathrm{fail}|S,H_B) = \int p(\mathrm{fail}|S,h,H_B) f_H(h) dH \tag{4}$$

Eq. (4) was evaluated for each time step in the *SWAN + ADCIRC* simulation and the maximum failure probability value was used to assess bridge vulnerability. For each bridge, the relationship between probability of failure and depth of inundation was described by a characteristic S-curve. This follows from the sigmoidal nature of the logistic function in Eq. (2). A feature of this relationship is that for a small increase in inundation, there may be a sharp rise in failure probability. The fragility model described in Eqs. (2)–(4) can only be used to calculate the failure probability of simply supported spans via bridge deck unseating. This support condition is typical of the main spans for a majority of the bridges in the case study region and all of the approach spans.

Results

Of the 25 bridges examined, six exhibited a probability of failure greater than 10%. Therefore further analysis and discussion is limited to these bridges. Bridges 10 and 11 and Bridges 13 and 14 are colocated bridge pairs that serve as the only evacuation and reentry routes for their corresponding island communities. Bridge 10 is located along State Highway 332 and spans the Intracoastal Waterway between Freeport and the island community of Surfside, whereas Bridge 11 serves as a feeder road to Bridge 10

Table 3. Maximum Roadway Inundation Depths (m) for Each Landscape, Sea Level, and Storm Scenario

Bridge	S_B	S_{FM}	S_{FM+SLR}	M_B	M_{FM}	M_{FM+SLR}	L_B	L_{FM}	L_{FM+SLR}	XL_B	XL_{FM}	XL_{FM+SLR}
10	2.38	2.46	2.74	3.37	3.37	3.65	3.83	3.81	4.07	4.24	4.23	4.51
11	2.36	2.43	2.72	3.34	3.35	3.62	3.79	3.78	4.04	4.22	4.20	4.49
13	0.84	0.85	1.11	1.53	1.56	1.81	1.77	1.81	2.10	2.35	2.38	2.69
14	2.09	2.11	2.36	2.78	2.81	3.06	3.03	3.07	3.35	3.60	3.63	3.94
15	0.51	0.55	0.81	1.52	1.51	1.76	1.69	1.68	1.92	2.21	2.21	2.45
25	2.31	2.42	2.71	3.32	3.34	3.64	3.85	3.85	4.16	4.52	4.53	4.87

Note: B = baseline; FM = future morphology; FM + SLR = future morphology with sea-level rise; L = large; M = medium; S = small; XL = extra-large.

(Fig. 1). Similarly, Bridge 14 is located on Farm-to-Market Road 1495 connecting Freeport to Bryan Beach and the island community of Quintana, whereas Bridge 13 serves as the feeder road to Bridge 14. The remaining bridges are located farther inland. Bridge 15 connects Highway 523 across the Dow Bridge Canal and serves as an evacuation route for the City of Freeport and a means of access to several industrial facilities. Bridge 25 is located along Redfish Drive approximately 16 km northeast of Freeport in a community located along Bastrop Bayou. This bayou is hydraulically connected to the coast through Bastrop Bay via San Luis Pass, a tidal inlet located at the northeast end of Follets Island. Bridge 25 is the sole access point to this island residential community.

Hydrodynamics at Bridge Locations

Fig. 3 shows the evolution of storm surge in time at each bridge location (column) and for each storm intensity (row), landscape, and sea-level scenario (line type). Roadway inundation depth, or alternatively stage, represents the still-water elevation of the storm and excludes changes to the free surface due to wave action. Bridges 10 and 11 and Bridges 13 and 14 are represented jointly due to their close proximity and similarity in stage hydrographs. After solution of the generalized wave continuity equations, but prior to solution of the momentum equations (within the middle of the time loop), *ADCIRC* implements a wetting and drying algorithm that regulates participation of each node in further computations by comparing water levels against a minimum wetness height. Although the *ADCIRC* wetting and drying algorithm is inherently more complex than explained herein (Dietrich et al. 2004), for consistent bottom friction, a node transitions from dry to wet once an adjacent node reaches a threshold free surface elevation such that the gradient allows water to flow into the element of interest. This threshold free surface elevation gradient is represented in *ADCIRC* as a minimum wetting velocity and was chosen for this study to be 0.01 m/s. Similarly, a node transitions from wet to dry once the total water depth drops below a nominal water depth, which was chosen for this study to be 0.10 m. These criteria were surpassed at low-lying roadways (Bridges 10, 11, and 25) 42 h prior to storm landfall. For elevated roadways (Bridges 13, 14, and 15), the target elements became wet 1–2 h prior to landfall.

There is a direct correlation between maximum roadway inundation depth and storm intensity (Fig. 3). This observation should be intuitive, and supports the supposition that the IKE is a first-order proxy for storm surge generation potential. The sensitivity of stage hydrographs to changes in coastal morphology and SLR (FM + SLR), i.e., the future scenario, varies spatially and with roadway elevation. For the majority of low-lying roadways (Bridges 10/11 and 25), there were two distinct modes of response that occurred: prelandfall and postlandfall. Prior to storm landfall, the stage at both bridges increased monotonically along the rising limb of the hydrographs [Figs. 3(a and b)]. To isolate the contribution of SLR to this trend, landscape changes were simulated independently (FM). From Figs. 3(a and b), it is evident that SLR dictated the hydrodynamic response at both bridges prior to storm landfall, for all storm intensities, with morphologic changes (FM) only slightly (<0.1 m) elevating inundation levels above baseline. This was also the case for the elevated roadways at Bridges 13/14 and 15.

After storm landfall, landscape changes appeared to regulate the impact of SLR on roadway inundation. This was most obvious along the falling limb of the stage hydrograph for Bridges 10/11 [Fig. 3(a)]. Beginning with the smallest storm, morphologic changes (FM) resulted in only a slight decrease (~0.1 m) in inundation depths from baseline conditions, and therefore SLR (FM + SLR) was again the primary contributor to the ~0.2 m increase in stage over baseline. However, as the storm intensity increased, stage continued to decrease due to morphologic changes until SLR was nearly completely offset, as documented for the results of the XL storm. This trend was also produced for the elevated roadways at Bridges 13/14 and 15 for the XL storm, although to a lesser extent due to lower stage elevations. Additionally, Table 3 highlights that the increase in maximum roadway inundation for the future scenario (FM + SLR) was approximately equivalent (±0.10 m) to the SLR value incorporated into *SWAN + ADCIRC* (0.31 m). As modeled for Bridge 25 [Fig. 3(b)], storm simulation postlandfall was limited due to the temporal resolution of the wind fields, and therefore the full descending limb of the stage hydrograph was not captured. The source of this extended lag time is detailed in the "Discussion" section.

Fig. 4 shows the time of roadway inundation, which represents the time base of the stage hydrographs depicted in Fig. 3 above the 0.6 m accessibility threshold (black line) for each simulation. Low-lying bridges (Bridges 10, 11, and 25) remained inundated, and therefore impassable, for the longest time, approaching the total simulation duration (69 h) for the FM + SLR scenario. Interestingly, for coastal bridges [Figs. 4(a and c)], landscape changes (FM) reduced the time that the roadway remained inundated during the larger intensity storms (L and XL), damping the effect of SLR for the future scenario (FM + SLR). For inland bridges, landscape changes (FM) either increased [Fig. 4(b)] or produced no change [Fig. 4(d)] in inundation time.

Regional Impact of Landscape Change and SLR

From the stage hydrographs, it is difficult to ascertain the additional storm surge elevation at roadways induced by landscape changes at the coast. To elucidate the impact of landscape change on the propagation of storm surge inland, volumetric flow was computed for each time-step across transects encompassing the coastal landscape modifications. The resulting time series are shown in Fig. 5, where negative flow corresponds to landward-directed flow and positive flow to seaward-directed flow. Figs. 5(a and b) depict the net flow across Transect 1 (Brazos River delta) and Transect 2 (Follets Island), respectively, for the baseline scenario. The baseline trend in volumetric flow at each transect did not vary significantly with changes in storm intensity. However, the magnitude of flow

Nat. Hazards Rev., 2018, 19(1): 04017020

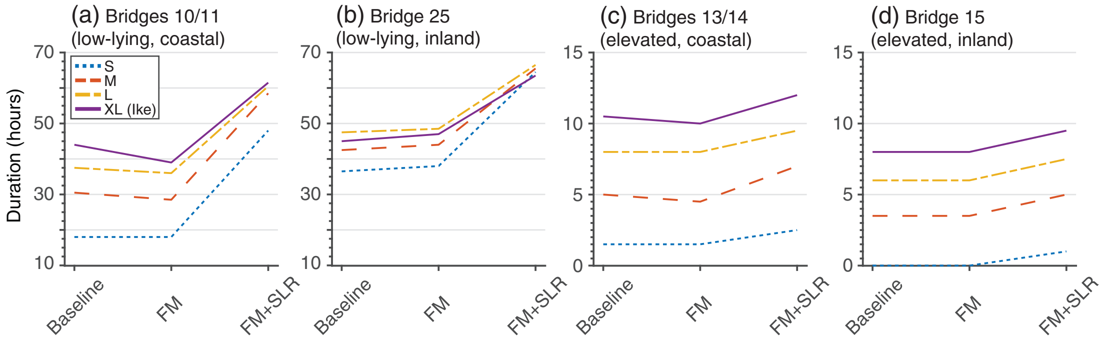

Fig. 4. (Color) Time of roadway inundation, representing stage above 0.6 m (accessibility threshold), and sea level scenarios at bridge locations (a–d), for each storm intensity (color)

landward (prior to landfall) and seaward (postlandfall) increased with storm intensity for both transects. The flow reversal at storm landfall corresponded well with previous observations of storm hydrodynamics along the UTGC for hurricanes striking the coast perpendicular to the shoreface (Rego and Li 2010).

The difference in volumetric flow between the FM + SLR and baseline scenarios [Figs. 5(c and d)] was calculated to depict where and how the future scenarios deviate from the baseline [Figs. 5(a and b)]. For example, in Fig. 5(c), a negative difference prior to storm landfall corresponds to an increase in landward-directed flow. Similarly, a positive difference after landfall corresponds to an increase in seaward flow. Figs. 5(c and d) show that with one exception [denoted with a box in Fig. 5(d) and elaborated upon in the "Discussion"], there was a net increase in the inflow and outflow of surge water over baseline conditions at both transects prelandfall and postlandfall, respectively. At Transect 1 (Brazos River delta), the increase in volumetric flow increased with storm intensity. This was also the case for the increase in outflow postlandfall at Transect 2. In contrast, the increase in inflow, or more precisely storm surge overtopping, immediately prior to landfall at Transect 2 (Follets Island) was significant for small storms (1,000–7,000 m^3/s), but decreased with increasing storm size. Figs. 5(e and f) show the relative contribution of SLR to the changes in volumetric flow depicted for the future scenario (FM + SLR) in Figs. 5(c and d). Along Transect 1, the increase in sea level contributed a maximum of ~2,500 m^3/s to net inflow (large-intensity storm), with negligible contributions to outflow postlandfall. For Transect 2, the impact of SLR on volumetric flow was more pronounced, particularly through the increase in outflow for the synthetic storms (S, M, and L), which exceeded 7,500 m^3/s for the large-intensity storm.

To assess the impact of SLR and landscape changes on wave height and the pattern of wave propagation, the difference

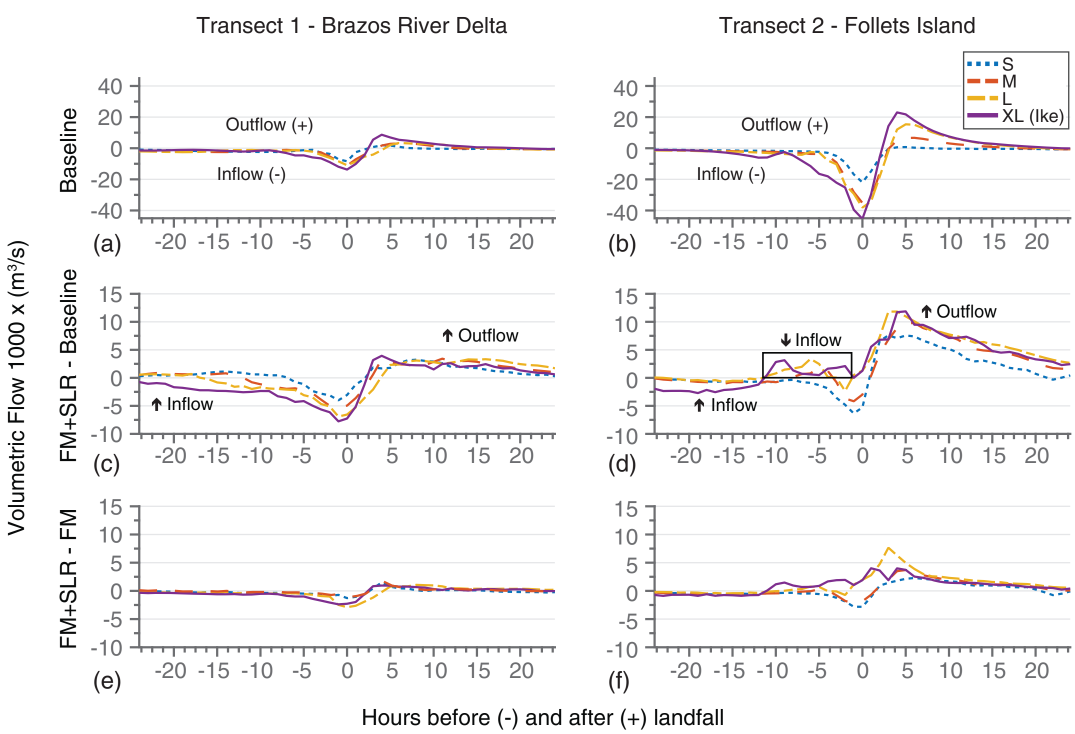

Fig. 5. (Color) Time series indicating volumetric flow across transects encompassing landscape modifications to (a) the Brazos River delta (Transect 1); (b) Follets Island for the baseline scenario; the direction of flow in (a) and (b) is landward (−) prior to landfall and seaward (+) postlandfall; the difference in volumetric flow between the future (FM + SLR) and baseline scenarios is depicted in (c) and (d); the relative contribution of SLR to the changes in volumetric flow is shown in (e) and (f); in (c–f), a negative difference prior to storm landfall corresponds to an increase in landward-directed flow between scenarios; similarly, a positive difference after landfall corresponds to an increase in seaward flow

Nat. Hazards Rev., 2018, 19(1): 04017020

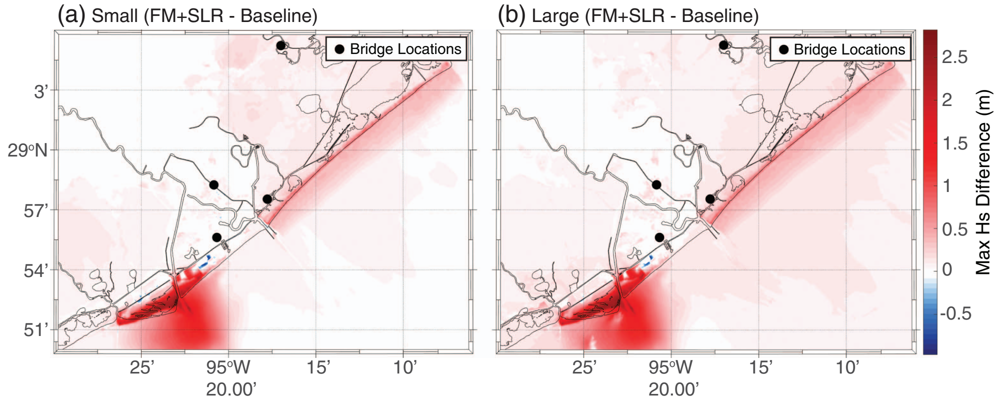

Fig. 6. (Color) Difference in maximum significant wave height (m) between the future (FM + SLR) and baseline scenarios for the (a) small and (b) large intensity storms

in maximum significant wave height between the FM + SLR and baseline scenarios is determined (Fig. 6). For simplicity, only small-intensity and large-intensity storms are depicted in Fig. 6. However, wave propagation patterns mirrored maximum still-water inundation extents (not shown), and therefore the spatial extent of wave propagation inland increased with storm intensity. Wave heights were amplified at the coast along both landscape changes, with the greatest increases observed along the eroded foredune of Follets Island (0.5–1.0 m) and the entire subaqueous delta plain of the Brazos River delta (1.0–2.8 m). There was also wave growth (<0.4 m) in back bays and along coastal floodplains outside of the Freeport storm protection system because waves propagated farther inland. Wave heights were reduced in a few isolated pockets, particularly in proximity to the river delta.

Probability of Bridge Failure

The probability of structural failure, via bridge deck unseating, under surge and wave loads was calculated at each bridge for all scenarios. In general, results showed that failure probability increased with storm surge and wave height and therefore storm intensity (Figs. 7 and 8). From Table 3 and Fig. 3, the maximum depth of inundation occurred at Bridge 25, which corresponds to the highest failure probability in Fig. 7. The difference in failure probabilities between Bridges 13 and 14 was due to a 1.25 m difference in roadway elevation, which produced an equivalent increase in storm surge at Bridge 14. However, bridge characteristics (Table 2), specifically the bridge deck elevation [H_B—a key parameter in Eq. (4)], produced the large-scale differences in failure probabilities between bridges with similar storm surge elevations. For example, although Bridges 25 and 10/11 are both low lying (0.288–0.362 m AMSL) and exhibit similar maximum depths of inundation (±0.38 m), the failure probability for Bridge 25 was nearly triple that for Bridges 10/11.

Interestingly, with the exception of Bridges 13 and 15, all bridges approached certain failure for the XL storm (Hurricane Ike) despite low to moderate initial failure probabilities for the small storm. In Fig. 7, the increase in storm surge height due to SLR was the

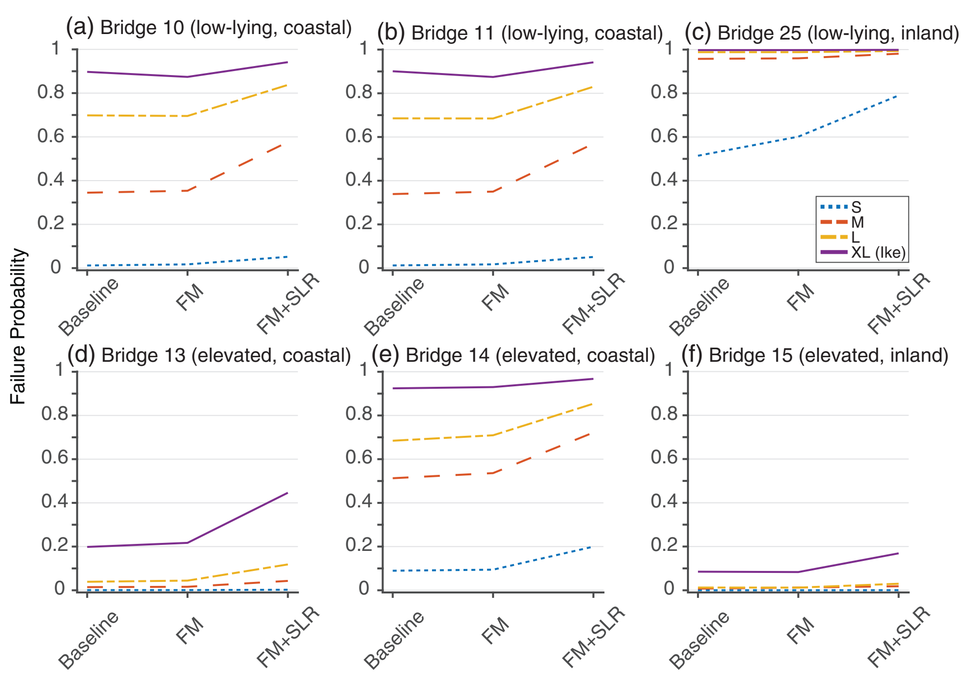

Fig. 7. (Color) Failure probability at select bridges (a–f) for each storm intensity (color) and landscape scenario

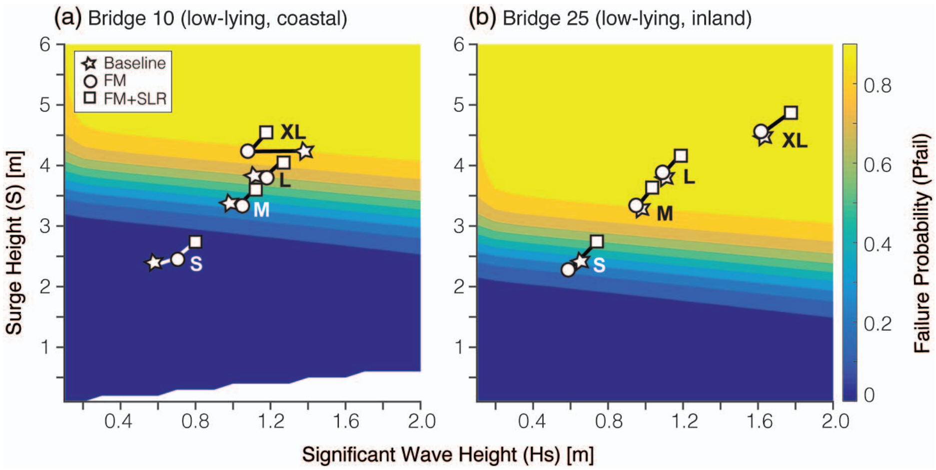

Fig. 8. (Color) Plan view of the characteristic S-shape fragility curves for Bridges 10 and 25 given a range of maximum inundation depths and significant wave heights

primary contributor to the increase in failure probability for the future scenario (FM + SLR), because changes to morphology (FM) only slightly elevated failure probabilities above baseline at each bridge. This result can be explained through the characteristic S shape of the fragility curves, which are shown in planform for Bridges 10 and 25 in Fig. 8. With the exception of Bridge 25, all bridges exhibited a baseline failure probability for the small storm that fell along the lower portion of the rising limb of the S curve [e.g., dark blue in Fig. 8(a)]. For these bridges, failure probability rose sharply with storm surge and wave height, and thus SLR, although seemingly small (0.31 m), significantly increased the fragility of bridge approach spans. For Bridge 25, the baseline failure probability was moderately high for the small storm, and therefore a small increase in storm surge, whether by storm intensity or SLR, propelled the failure probability to the asymptotic limit [Fig. 8(b)].

Discussion

This paper represents a multidisciplinary effort to provide an integrative model of the combined effects of rising seas and changing coastal landscapes on the vulnerability of highway bridges to extreme storms. Storm surge impacting the Freeport region has the potential to cause large-scale economic and environmental damage. Hurricane Ike illuminated the vulnerability of coastal infrastructure along the UTGC and provided a wealth of empirical evidence of bridge damages and failure modes. For example, the Pelican Island Bridge, a major highway bridge that spans the Intracoastal Waterway in Galveston, Texas, experienced severe erosion along its approaches, with repair costs exceeding \$6.5 million (Elder 2010). The magnitude of such damages inspired the development of new fragility models capable of quantifying the risk of damage from storm surge and wave loading (Kameshwar and Padgett 2014). The research presented in this study demonstrates the importance of incorporating future projections of landscape change when assessing the impacts of climate change and SLR on bridge reliability, and most notably, the prehurricane and posthurricane accessibility of critical infrastructure.

Relative sea-level rise increases bridge vulnerability by enhancing wave and surge loads, with landscape changes only slightly elevating failure probabilities above the baseline (Fig. 7). The effect of landscape change on bridge accessibility is more complex, varying spatially with storm size and bridge characteristics. For small-intensity storms, storm surge levels are relatively low and the system responds to the increase in sea level and landscape modifications through an increase in overland flooding. This result should not be surprising, because SLR introduces more water into the system and erosional modifications to the coastline allow this water to more easily bypass natural barriers. Enhanced flooding of back bays led to an increase in inundation time at low-lying bridges (e.g., Bridges 10 and 11) by 25 h prior to landfall and 5 h postlandfall (Figs. 3 and 4).

As storm intensity increases, integrated feedback mechanisms between coastal morphology and hydrodynamics begin to regulate the impact of SLR on bridge reliability. The observed decrease in inflow across Follets Island approximately 10 h prior to landfall for the M–XL intensity storms [Fig. 5(d)] can be explained through infilling of the back-barrier bay. Upon closer inspection of the still-water elevation (color) and direction of flow (velocity vector) at this time, there is clearly a seaward-directed gradient in water

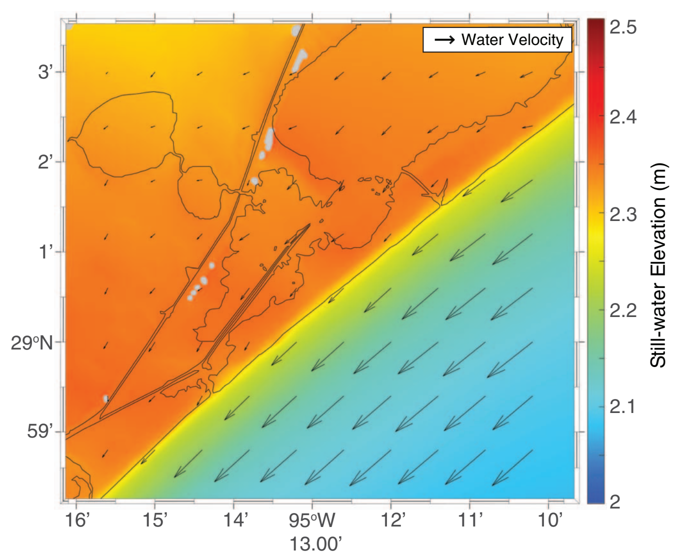

Fig. 9. (Color) Seaward-directed flow (velocity vectors, m/s) prior to hurricane landfall across the deflated barrier island due to infilling of the back-barrier bay, which creates a seaward-directed gradient in still-water levels (color); areas in gray are associated with dry nodes (0-m still-water elevation)

levels prior to landfall (as shown in Fig. 9 for the southwest portion of Transect 2). This phenomenon can be attributed to strong shore-parallel currents and winds, which elevate back-bay water levels sufficiently to surpass the elevation of the barrier island prior to landfall, thereby forcing water seaward. During Hurricane Ike, a forerunner surge, driven by shore-parallel winds acting on the large and shallow continental shelf, led to a similar early rise in water levels in coastal bays (Hope et al. 2013; Kennedy et al. 2011; Sebastian et al. 2014). However, the landscape modifications modeled in this study, specifically erosion of the barrier island dune ridge, serve to enhance this seaward-directed gradient. This phenomenon, in conjunction with the increase in outflow of storm surge ebb due to deflation of the barrier island [Figs. 5(d and f)], lowers the roadway inundation time at coastal bridges after storm landfall (Fig. 4). In terms of bridge performance, if coastal bridges do not fail completely due to hurricane loading (Figs. 7 and 8), then barrier deflation is determined to be beneficial, because it offsets the poststorm effects of SLR, thus enabling coastal bridges to become accessible for rescue and recovery operations up to an hour earlier than present-day estimates (Fig. 3). This result highlights the importance of using a holistic approach when modeling SLR, because a static increase in water level would otherwise overestimate bridge inundation times by neglecting significant back-barrier interactions. Although counterintuitive, these results also illustrate that low-lying barriers can prolong coastal flooding in back-bay floodplains. However, storm-induced breaching, which was documented at over 75 locations along Follets Island after Hurricane Ike (Harter et al. 2015), was not modeled in this study and would likely significantly aid in the present-day poststorm draining of flood water from back-bay regions.

For Bridge 25, which is located along an inland bayou and hydraulically connected to the coast through Bastrop Bay via San Luis Pass (Fig. 1), the aforementioned benefit of barrier island erosion for reducing inundation time is less evident because of backwater effects. Here, water level is a function of channel hydraulics and overland flow; enhanced overtopping of the barrier island due to SLR serves to elevate water levels within back-bays and thus creates backwater on connecting bayous. This effect would likely be amplified by rainfall runoff, which was not incorporated into the $SWAN + ADCIRC$ model. However, the vulnerability of Bridge 25 lies primarily in its construction details because even for small storms the bridge is highly vulnerable to wave and surge loading (Fig. 8). At Bridge 25, the synthetic storms (S, M, and L) produced an increase in inundation time with increasing storm intensity, whereas Hurricane Ike (XL) deviated from this trend [Fig. 4(b)]. Thus although the chosen synthetic storms appeared to produce similar hydrodynamic trends to the historical storm at bridges near the coast, complexities may exist as the synthetic storms propagate inland.

The modeled erosion of the Brazos River delta did not affect the performance of adjacent bridges in terms of deck unseating probability and inundation duration. However, the impacts of this landscape modification to coastal flooding were significant. This is clear, for example, through the increase in inflow of 7,500 m^3/s for the future scenario XL storm [Fig. 5(c)], of which only 2,400 m^3/s can be attributed to SLR [Fig. 5(e)]. Maximum significant wave height was also amplified by up to 2.8 m along the eroded deltaic plane, which can be attributed to slightly more wave growth and less wave dissipation.

Because of the reducing effect of the modeled landscape changes (particularly deflation of the barrier island foredune) on inundation times for the M, L, and XL storms, the relative impact of SLR on bridge accessibility was greatest for low-lying coastal bridges during small intensity storms. At Bridges 10 and 11, elevated storm surge levels led to a 30-h increase in total inundation time for the small storm and a 17-h increase for the XL storm for the future scenario. This result illuminates the vulnerability of infrastructure to coastal change; despite only a modest increase in sea level (0.31 m), the surge response rendered Bridges 10 and 11 impassable for one extra day. For evacuation planning purposes, coastal communities that rely on low-lying bridges as the primary route will need to evacuate more than 40 h in advance of hurricane landfall, regardless of storm intensity, to avoid submerged roadways (Fig. 3). Thus the risk that SLR and landscape changes pose for potential loss of life due to a reduction in infrastructure functionality, in terms of impeded accessibility due to water inundation, is substantial. This risk is further compounded by increased bridge structural failure probability due to intensified wave and surge loading.

Conclusion

This illustration of a coupled hydrodynamic, geomorphic, and engineering reliability modeling framework demonstrates a novel approach for studying the interaction between environmental change and infrastructure vulnerability. The developed methodology was applied to a portfolio of bridges in Freeport, Texas, a low-lying and storm-prone region located along the UTGC. A hurricane storm surge and wave model representing present-day conditions was modified to represent potential landscape changes associated with a regional rise in sea level of 0.31 m, an intermediate scenario for the year 2050. Landscape changes, including the erosion and landward migration of a barrier island, and the erosion of a subaqueous deltaic plain, were developed by extrapolating historical trends and geometric relationships. Four storms, of both synthetic and historical origin, were used to simulate water levels and wave heights at critical bridge locations in the region. The spatial and temporal trends in roadway inundation were examined and used for comparison of maximum inundation depths and time of inundation between scenarios. Changes in volumetric flow and significant wave height were analyzed across the modeled landscape changes to relate the hydrodynamics observed at bridge locations to trends at the coast. This analysis then informed a bridge reliability assessment, which incorporated both bridge accessibility and structural fragility, to infer the safety and longevity of transportation infrastructure susceptible to extreme storm events in a changing climate and coastal landscape.

Bridge structural vulnerability was found to increase with storm surge and wave height, and therefore storm intensity, as well as sea level. This result was expected from analytic relationships and previous numerical studies. The impact of landscape changes on surge and wave loads was negligible and only slightly elevated failure probabilities above baseline conditions.

The impact of landscape changes on bridge accessibility was more complex; barrier erosion and transgression can increase, decrease, or produce no change in inundation times for storms of different intensity due to changes in wind-setup and back-bay interactions. Strong shore-parallel winds associated with medium-intensity to extra-large–intensity storms initiated a seaward-directed flux of floodwaters across the deflated barrier island prior to storm landfall. This prelandfall draining of the back-bays, in conjunction with an increase in outflow of storm surge ebb due to deflation of the barrier island, lowered total inundation time for the 2050 scenario at adjacent low-lying bridges by up to 5 h for the largest-intensity storm. When evaluating just the postlandfall inundation time for these bridges, barrier island deflation was determined to be beneficial because it offsets the poststorm flood elevation caused by the rise in sea level. This could enable coastal bridges to become accessible for rescue and recovery operations for the 2050 scenario up to 1 h earlier than present-day estimates.

The reducing effect of future landscape change on inundation time was not observed for small intensity storms. Therefore the relative impact of SLR on bridge accessibility was found to be greatest for low-lying bridges during small-intensity storms. For the lowest-lying bridges evaluated in this study, elevated storm-surge levels associated with the 0.31-m SLR led to a 30-h increase in total inundation time for the small storm versus a 17-h increase for the XL storm for the 2050 scenario.

For all the bridges analyzed in this study, structural failure probability was linked to a reduction in clearance due to an increase in sea level, storm surge, and wave height. These results suggest that raising low-lying main spans may enhance efforts aimed at protecting critical infrastructure. Elevating approach spans is generally not feasible; however, resistance against unseating could be improved by tying the approach span to the bridge substructure. Tie-downs should be designed so that they do not induce failure of the substructure or negative bending (FHWA 2016). Future work should address fragility modeling of bridges with retrofits or alternative design details such as tie-downs as prospective measures to improve the resistance to bridge deck unseating and reduce vulnerability in current or future climate conditions.

Although the vulnerability analysis performed in this study was based on scenario storm events across a range of intensity, the use of storms representative of design recurrence intervals or analysis of suites of synthetic storms would support risk assessment across a region. Furthermore, although there is inherent uncertainty in how the landscape will change in response to SLR, this study highlights the importance of incorporating projected changes in infrastructure vulnerability analysis. This is particularly important in regions with back-barrier bays where the potential for nonlinear interactions with SLR is high. Future work should consider the inclusion, and concurrent occurrence, of other types of bridge hazards such as scour, aging, and collision events involving debris. In addition, forward modeling that incorporates the processes that contribute to landform changes (Lorenzo-Trueba and Ashton 2014; Masetti et al. 2008) or probabilistic predictions of landscape change (Bilskie et al. 2016b; Gutierrez et al. 2015; Passeri et al. 2016; Plant et al. 2016) should be used to better constrain future morphodynamic change. Although this study used only a single SLR scenario, risk management planners should simulate a range of sea levels and storm characteristics (e.g., angle of approach, track, and forward speed) to project coastal flooding under a variety of potential climate change and storm scenarios.

Acknowledgments

This research was supported by the Shell Center for Sustainability at Rice University through funding to the grant Stress Nexus of Coastlines: Population Development, Infrastructure Security, and Morphological Dynamics of the Upper Texas Gulf Coast; and by the Houston Endowment under the Severe Storm Prediction, Education, and Evacuation from Disasters (SSPEED) Center. The authors also acknowledge the support of Dr. Clint Dawson and the Texas Advanced Computing Center for the use of their computing resources.

References

ArcGIS [Computer software]. ESRI, Redlands, CA.

Ataei, N., and Padgett, J. E. (2013). "Probabilistic modeling of bridge deck unseating during hurricane events." *J. Bridge Eng.*, 10.1061/(ASCE)BE.1943-5592.0000371, 275–286.

Atkinson, J., Smith, J. M., and Bender, C. (2013). "Sea-level rise effects on storm surge and nearshore waves on the Texas coast: Influence of landscape and storm characteristics." *J. Waterw. Port Coastal Ocean Eng.*, 10.1061/(ASCE)WW.1943-5460.0000187, 98–117.

Bass, B., Irza, J. N., Proft, J., Bedient, P., and Dawson, C. (2017). "Fidelity of the integrated kinetic energy factor as an indicator of storm surge impacts." *Nat. Hazards*, 85(1), 575–595.

Bilskie, M. V., et al. (2016a). "Dynamic simulation and numerical analysis of hurricane storm surge under sea level rise with geomorphologic changes along the northern Gulf of Mexico." *Earth's Future*, 4(5), 177–193.

Bilskie, M. V., Hagen, S. C., Medeiros, S. C., Cox, A. T., Salisbury, M., and Coggin, D. (2016b). "Data and numerical analysis of astronomic tides, wind-waves, and hurricane storm surge along the northern Gulf of Mexico." *J. Geophys. Res. Oceans*, 121(5), 3625–3658.

Bilskie, M. V., Hagen, S. C., Medeiros, S. C., and Passeri, D. L. (2014). "Dynamics of sea level rise and coastal flooding on a changing landscape." *Geophys. Res. Lett.*, 41(3), 927–934.

Carlin, J., Dellapenna, T., and Figlus, J. (2015). "Investigating morphological and stratigraphic changes to the submarine shoreface of a transgressive barrier Island: Follets Island, northern Gulf of Mexico." *Coastal Sediments: Proc., Coastal Sediments*, World Scientific, Singapore.

Cazenave, A., and Cozannet, G. L. (2014). "Sea level rise and its coastal impacts." *Earth's Future*, 2(2), 15–34.

Church, J. A., et al. (2013). "Sea level change." *Climate change 2013: The physical science basis*, T. F. Stocker, et al., eds., Cambridge University Press, Cambridge, U.K.

Cobell, Z., Zhao, H., Roberts, H. J., Clark, F. R., and Zou, S. (2013). "Surge and wave modeling for the Louisiana 2012 coastal master plan." *J. Coastal Res.*, 67, 88–108.

Dawson, C., Kubatko, E. J., Westerink, J. J., Trahan, C., Mirabito, C., Michoski, C., and Panda, N. (2011). "Discontinuous Galerkin methods for modeling hurricane storm surge." *Adv. Water Resour.*, 34(9), 1165–1176.

DeConto, R. M., and Pollard, D. (2016). "Contribution of Antarctica to past and future sea-level rise." *Nature*, 531(7596), 591–597.

Dietrich, J. C., et al. (2011). "Modeling hurricane waves and storm surge using integrally-coupled, scalable computations." *Coastal Eng.*, 58(1), 45–65.

Dietrich, J. C., et al. (2013). "Real-time forecasting and visualization of hurricane waves and storm surge using $SWAN + ADCIRC$ and FigureGen." *Computational challenges in the geosciences*, C. Dawson and M. Gerritsen, eds., Springer, New York, 49–70.

Dietrich, J. C., Kolar, R. L., and Luettich, R. A. (2004). "Assessment of ADCIRC's wetting and drying algorithm." *Developments Water Sci.*, 55(Part 2), 1767–1778.

Ding, Y., Nath Kuiry, S., Elgohry, M., Jia, Y., Altinakar, M. S., and Yeh, K.-C. (2013). "Impact assessment of sea-level rise and hazardous storms on coasts and estuaries using integrated processes model." *Ocean Eng.*, 71, 74–95.

Elder, L. (2010). "Feds commit $6.5M to Pelican Island Bridge repairs." *The Galveston County Daily News*, May 2, 2010.

Elfrink, B., Hanes, D. M., and Ruessink, B. G. (2006). "Parameterization and simulation of near bed orbital velocities under irregular waves in shallow water." *Coastal Eng.*, 53(11), 915–927.

Federal Highway Administration. (2016). "Sea level rise and storm surge impacts on a coastal bridge: I-10 Bayway, Mobile Bay, Alabama." *FHWA-HEP-17-014*, Washington, DC.

FEMA and USACE (U.S. Army Corps of Engineers). (2011). "Flood insurance study: Coastal counties, Texas." *Intermediate submission 2: Scoping and data review*, Washington, DC.

Ferreira, C. M., Irish, J. L., and Olivera, F. (2014). "Uncertainty in hurricane surge simulation due to land cover specification." *J. Geophys. Res. Oceans*, 119(3), 1812–1827.

FitzGerald, D. M., Fenster, M. S., Argow, B. A., and Buynevich, I. V. (2008). "Coastal impacts due to sea-level rise." *Annu. Rev. Earth Planet. Sci.*, 36(1), 601–647.

Fraticelli, C. M. (2006). "Climate forcing in a wave-dominated delta: The effects of drought–flood cycles on delta progradation." *J. Sediment. Res.*, 76(9), 1067–1076.

Gibeaut, J. C., Waldinger, R., and Hepner, T. (2003). "Changes in bay shoreline position, West Bay System, Texas." *Rep. to the Texas Coastal Coordination Council and the General Land Office*, Bureau of Economic Geology, Univ. of Texas at Austin, Austin, TX.

Gulf Coast Community Protection and Recovery District. (2016). "Storm surge suppression study phase 3 report—Recommended actions." Houston.

Gutierrez, B. T., Plant, N. G., Thieler, E. R., and Turecek, A. (2015). "Using a Bayesian network to predict barrier island geomorphologic characteristics." *J. Geophys. Res.: Earth Surf.*, 120(12), 2452–2475.

Harter, C., Figlus, J., and Dellapenna, T. (2015). "The role of hurricanes on the morphological evolution of a sediment-starved barrier island along the Upper Texas Coast: Follets Island." *Proc., Coastal Sediments*, World Scientific, Singapore.

Hope, M. E., et al. (2013). "Hindcast and validation of Hurricane Ike (2008) waves, forerunner, and storm surge." *J. Geophys. Res*, 118(9), 4424–4460.

Huff, S. (2015). "Modeling the influence of large woody debris on delta morphology and longshore sediment transport using the Brazos delta." Master's thesis, Rice Univ., Houston.

Irish, J. L., Resio, D. T., and Ratcliff, J. J. (2008). "The influence of storm size on hurricane surge." *J. Phys. Oceanogr.*, 38(9), 2003–2013.

Kameshwar, S., and Padgett, J. E. (2014). "Multi-hazard risk assessment of highway bridges subjected to earthquake and hurricane hazards." *Eng. Struct.*, 78, 154–166.

Kennedy, A. B., et al. (2011). "Origin of the hurricane Ike forerunner surge." *Geophys. Res. Lett.*, 38(8), 1–5.

Lorenzo-Trueba, J., and Ashton, A. D. (2014). "Rollover, drowning, and discontinuous retreat: Distinct modes of barrier response to sea-level rise arising from a simple morphodynamic model." *J. Geophys. Res.*, 119(4), 779–801.

Luettich, R. A., and Westerink, J. J. (2004). *Formulation and numerical implementation of the 2D/3D ADCIRC finite element model version 44.XX*, Univ. of North Carolina at Chapel Hill, Morehead City, NC.

Masetti, R., Fagherazzi, S., and Montanari, A. (2008). "Application of a barrier island translation model to the millennial-scale evolution of Sand Key, Florida." *Cont. Shelf Res.*, 28(9), 1116–1126.

Morton, R. A., Miller, T., and Moore, L. (2005). "Historical shoreline changes along the US Gulf of Mexico: A summary of recent shoreline comparisons and analyses." *J. Coastal Res.*, 21(4), 704–709.

Morton, R. A., Miller, T. L., and Moore, L. J. (2004). *National assessment of shoreline change. Part 1: Historical shoreline changes and associated coastal land loss along the U.S. Gulf of Mexico*, Diane Publishing, Collingdale, PA, 1–45.

Mousavi, M. E., Irish, J. L., Frey, A. E., Olivera, F., and Edge, B. L. (2011). "Global warming and hurricanes: The potential impact of hurricane intensification and sea level rise on coastal flooding." *Clim. Change*, 104(3–4), 575–597.

National Weather Service. (2016). "Turn around don't drown." ⟨http://www.nws.noaa.gov/os/water/tadd/⟩ (Apr. 4, 2016).

Neumann, B., Vafeidis, A. T., Zimmermann, J., and Nicholls, R. J. (2015). "Future coastal population growth and exposure to sea-level rise and coastal flooding—A global assessment." *PLoS One*, 10(3), e0118571.

NOAA (National Oceanic and Atmospheric Administration). (2016). "Sea level trends." ⟨http://tidesandcurrents.noaa.gov/sltrends/sltrends.html⟩ (Apr. 2, 2016).

Odezulu, C. I., Lorenzo-Trueba, J., Wallace, D. J., and Anderson, J. B. (2017). "Stratigraphic and sedimentological evidence for unprecedented shoreline migration rate during historic time: Follets Island, TX." *Barrier dynamics and the impacts of climate change on barrier evolution*, L. J. Moore and A. B. Murray, eds., Springer, New York.

Padgett, J., DesRoches, R., Nielson, B., Yashinsky, M., Kwon, O.-S., Burdette, N., and Tavera, E. (2008). "Bridge damage and repair costs from Hurricane Katrina." *J. Bridge Eng.*, 10.1061/(ASCE)1084-0702(2008)13:1(6), 6–14.

Padgett, J. E., Spiller, A., and Arnold, C. (2012). "Statistical analysis of coastal bridge vulnerability based on empirical evidence from Hurricane Katrina." *Struct. Infrastruct. Eng.*, 8(6), 595–605.

Paine, J. G., Mathew, S., and Caudle, T. (2012). "Historical shoreline change through 2007, Texas Gulf Coast: Rates, contributing causes, and Holocene context." *Gulf Coast Assoc. Geol. Soc. J.*, 1, 13–26.

Park, Y. H., and Edge, B. L. (2011). "Beach erosion along the northeast Texas coast." *J. Coastal Res.*, 27(3), 502–514.

Parris, A., et al. (2012). "Global sea level rise scenarios for the United States National Climate Assessment." *NOAA Technical Rep. OAR CPO-1*, Climate Program Office, Silver Spring, MD.

Passeri, D. L., Hagen, S. C., Bilskie, M. V., and Medeiros, S. C. (2015a). "On the significance of incorporating shoreline changes for evaluating coastal hydrodynamics under sea level rise scenarios." *Nat. Hazards*, 75(2), 1599–1617.

Passeri, D. L., Hagen, S. C., Medeiros, S. C., Bilskie, M. V., Alizad, K., and Wang, D. (2015b). "The dynamic effects of sea level rise on low-gradient coastal landscapes: A review." *Earth's Future*, 3(6), 159–181.

Passeri, D. L., Hagen, S. C., Plant, N. G., Bilskie, M. V., Medeiros, S. C., and Alizad, K. (2016). "Tidal hydrodynamics under future sea level rise and coastal morphology in the Northern Gulf of Mexico." *Earth's Future*, 4(5), 159–176.

Plant, N. G., Thieler, E. R., and Passeri, D. L. (2016). "Coupling centennial-scale shoreline change to sea-level rise and coastal morphology in the Gulf of Mexico using a Bayesian network." *Earth's Future*, 4(5), 143–158.

Powell, M. D., and Reinhold, T. A. (2007). "Tropical cyclone destructive potential by integrated kinetic energy." *Bull. Am. Meteorol. Soc.*, 88(4), 513–526.

Ranasinghe, R., Callaghan, D., and Stive, M. J. F. (2012). "Estimating coastal recession due to sea level rise: Beyond the Bruun rule." *Clim. Change*, 110(3–4), 561–574.

Ratcliff, J., and Smith, J. M. (2012). *Sea level rise impacts to military installations in lower Chesapeake Bay*, ASCE, Reston, VA, 740–752.

Rego, J. L., and Li, C. (2010). "Storm surge propagation in Galveston Bay during Hurricane Ike." *J. Mar. Syst.*, 82(4), 265–279.

Rosati, J. D., Stone, G. W., Dean, R. G., and Kraus, N. C. (2006). "Restoration of barrier islands overlying poorly-consolidated sediments, south-central Louisiana." *Gulf Coast Assoc. Geol. Soc. Trans.*, 56, 727–740.

Schwartz, R. K. (1975). "Nature and genesis of some storm washover deposits." *Coastal Engineering Research Center Technical Memorandum No. 61*, U.S. Army Corps of Engineers, Washington, DC.

Sebastian, A., Proft, J., Dietrich, J. C., Du, W., Bedient, P. B., and Dawson, C. N. (2014). "Characterizing hurricane storm surge behavior in Galveston Bay using the *SWAN + ADCIRC* model." *Coastal Eng.*, 88, 171–181.

Smith, J. M., Cialone, M. A., Wamsley, T. V., and McAlpin, T. O. (2010). "Potential impact of sea level rise on coastal surges in southeast Louisiana." *Ocean Eng.*, 37(1), 37–47.

Stearns, M., and Padgett, J. E. (2011). "Impact of 2008 Hurricane Ike on bridge infrastructure in the Houston/Galveston region." *J. Perform. Constr. Facil.*, 10.1061/(ASCE)CF.1943-5509.0000213, 441–452.

Toro, G. R. (2008). *Joint probability analysis of hurricane flood hazards for Mississippi*, URS Group, Tallahassee, FL.

USACE (U.S. Army Corps of Engineers). (2005). *Freeport and vicinity, Texas hurricane-flood protection draft feasibility report*, Washington, DC.

USACE (U.S. Army Corps of Engineers). (2015). "Sea-level change curve calculator (2015.46)." ⟨http://www.corpsclimate.us/ccaceslcurves.cfm⟩ (Sep. 2, 2016).

Vickery, P. J., and Blanton, B. O. (2008). "North Carolina Coastal flood analysis system hurricane parameter development." *Renaissance Computing Institute Technical Rep. TR-08-06*, Univ. of North Carolina, Chapel Hill, NC.

Wallace, D. J., and Anderson, J. B. (2013). "Unprecedented erosion of the upper Texas coast: Response to accelerated sea-level rise and hurricane impacts." *Geol. Soc. Am. Bull.*, 125(5–6), 728–740.

Wallace, D. J., Anderson, J. B., and Fernández, R. A. (2010). "Transgressive ravinement versus depth of closure: A geological perspective from the upper Texas coast." *J. Coastal Res.*, 26(6), 1057–1067.

Wallace, D. J., Anderson, J. B., and Rodriguez, A. B. (2009). "Natural versus anthropogenic mechanisms of erosion along the upper Texas coast." *Geol. Soc. Am.*, 460, 137–147.

Wang, J., Gao, W., Xu, S., and Yu, L. (2012). "Evaluation of the combined risk of sea level rise, land subsidence, and storm surges on the coastal areas of Shanghai, China." *Clim. Change*, 115(3–4), 537–558.

Woodruff, J. D., Irish, J. L., and Camargo, S. J. (2013). "Coastal flooding by tropical cyclones and sea-level rise." *Nature*, 504(7478), 44–52.

Zervas, C., Gill, S., and Sweet, W. (2013). "Estimating vertical land motion from long-term tide gauge records." *NOAA Technical Rep. NOS CO-OPS 065*, U.S. Dept. of Commerce, Washington, DC.

Zhang, K., Li, Y., Liu, H., Xu, H., and Shen, J. (2013). "Comparison of three methods for estimating the sea level rise effect on storm surge flooding." *Clim. Change*, 118(2), 487–500.